Model-Based Optimization of the Operating Window for Electrophysical Silver Deposition Using a Dimensionless Regime Map

Abdimitalip Satybaldyev[1], Yslamidin Tashpolotov[2], Madina Sarybaeva[3] and Dilnaz Jolboldu[1]
[1]*Osh Technological University named after M. M. Adyshev, Nasirdin Isanov Str. 81, 723503 Osh, Kyrgyz Republic.*
[2]*Department of Experimental and Theoretical Physics, Osh State University, 331 Alymbek Datka Str. 331, 723500 Osh, Kyrgyz Republic.*
[3]*Kyrgyz-Uzbek International University named after Batyraly Sydykov, Gapar Aitiev Str. 27, 723500 Osh, Kyrgyz Republic.*
a.baatyrbekovich@gmail.com, itashpolotov@mail.ru, sarybaevamadina2409@gmail.com, jolboldukyzydilnaz@mail.com

Keywords: Nernst-Planck Model, Silver Ionization, Field Effects, Active Surface, Dimensionless Numbers.

Abstract: We present a quantitative characterization of the kinetics of silver deposition during electrophysical ionization (EPI), focusing on the roles of electric field strength E and interelectrode gap d. Series Δm(E) were obtained for d=1.5, 2, 3 cm. For small gaps, the yield exhibits a smooth, sigmoid-like increase followed by saturation (a plateau); at d=3 cm the curve becomes nonmonotonic - a pronounced maximum is followed by a decline - indicating a switch in the dominant mass-transfer step. The interpretation is developed within a steady-state formulation of the Nernst–Planck equations with a Robin (mixed) boundary condition at the cathode and a phenomenological "active-surface availability" factor η(E). It is shown that a decreasing η(E) adequately describes monotonic regimes, whereas for large d realistic reproduction of the peak and subsequent drop is achieved by introducing a peaked η(E) or a weak field dependence of the external mass-transfer coefficient $k_c(E)$. This behavioral shift is consistent with morphological evolution of the deposit - from a compact structure to a dendritic–porous one with a self-screening effect. The dimensionless drift parameter β=zFEd/RT and the Damköhler number Da=kcd/D define a regime map that orders the series by d and delineates the "operating window" for E. Practically, this implies maintaining the field near its optimum, providing gentle hydrodynamic mixing and thermal stabilization (particularly at d≥3 cm), and structurally suppressing field focusing. The results provide a basis for scaling EPI and for adaptive control of silver deposition.

1 INTRODUCTION

In many modern chemico-technological schemes one tries, almost inevitably, to solve two problems at once: to recover valuable metals and, at the same time, to clean the aqueous medium without relying on a constant stream of added reagents. This double task is now seen as a characteristic feature of "green" production routes rather than an optional improvement. Against this background, electrophysical ionization (EPI) stands out as a comparatively simple but promising option. In a usual EPI setup the operator really has only a few knobs to turn: mainly the electric field strength E and the interelectrode gap d; the liquid phase can remain chemically simple, and the hardware itself is compact and not overloaded with auxiliaries [1] - [4]. Such minimalism is attractive in practice, but it also means that we must understand much better how a particular pair (E, d) actually translates into a certain deposition rate and a measurable mass gain Δm. Without this understanding it is difficult to design robust processes or to think seriously about closed-loop control [4] - [6].

Silver is a convenient system on which to explore these questions. It is technologically important, its deposits are very sensitive to transport and kinetic conditions, and, from an experimental point of view, the mass gain can be followed by straightforward gravimetric measurements. When one performs series of experiments in flat-plate EPI cells, an interesting

pattern appears. The dependence of the deposited mass Δm on E at fixed d is not a simple straight rise. For small gaps $\Delta m(E)$ typically increases in a somewhat S-shaped fashion and then levels off, whereas for larger gaps the curve often shows a pronounced maximum and then begins to decline [5]. In other words, as the gap grows, the system "switches" from a monotonic saturation-type behavior to a bell-shaped one. This qualitative change suggests that the rate-limiting steps are no longer the same: electromigration, diffusion and surface morphology (roughness, porosity, partial passivation) start to interact in a different way. Under such conditions it is no longer true that simply increasing E yields more silver; beyond a certain point the effectively active surface shrinks, screening becomes important, and the marginal gain per unit field can even turn negative [5].

If we want to move from such qualitative statements to predictive tools, a purely heuristic discussion is not enough. A framework is needed in which ion transport and interfacial reaction are treated together, while morphology-related effects are taken into account in a form that is still manageable. From this point of view, steady-state one-dimensional formulations of the Nernst–Planck type are a natural starting point. Earlier studies have used such models, alongside mass-transfer-coefficient approaches, to analyze reactive transport under externally imposed electric fields and to compare alternative descriptions of ion exchange and deposition [7], [8]. However, these works are usually tied to specific reactor geometries or particular sorbent systems. They do not offer a compact, experimentally checked "regime map" that would organize the operating space of EPI directly in terms of E and d and provide simple, visual rules for selecting a suitable window of conditions [6] - [8].

A reasonable way to compress the complexity of the problem is to resort to nondimensional analysis. When the Nernst–Planck equation is combined with a mixed (kinetically limited) boundary condition at the cathode, two dimensionless groups appear in a very natural manner. One can identify a drift parameter β, which compares electromigration with diffusion, and a Damköhler number Da, which measures the competition between interfacial reaction and mass transport. Taken together, β and Da span a "regime plane" on which different qualitative behaviors of $\Delta m(E)$-from monotonic saturation to bell-shaped curves-can be located. If experimental data for EPI-driven silver deposition can be reliably mapped onto this (β, Da) plane, measurements obtained at different gaps should, at least to a large extent, collapse, and the transfer of operating conditions between geometries becomes more transparent [7], [9].

Of course, a continuum-level description on its own would be incomplete. Real electrodes are not smooth mathematical surfaces. Dendritic structures, porous layers and locally passivated patches strongly modify the effective active area and, therefore, the overall reaction rate. For this reason it is reasonable to introduce an "active-surface fraction" $\eta(E)$, which summarizes, in a compact form, how morphological evolution and field redistribution reduce the proportion of surface sites that participate in efficient deposition as E increases. Earlier work on electrochemically assisted ion-exchange and hybrid separation processes has shown that such reduced descriptions can remain both physically interpretable and practically useful, provided that they are linked back to experimental observations [1] - [3], [7], [8]. In the present study $\eta(E)$ plays precisely this bridging role: it connects a mathematically simple transport model with the kinetics that are actually observed on a morphology-evolving surface.

Verification at the microstructural level is, in this setting, not merely an illustration but a necessary part of the analysis. Micrographs of the deposited silver layers, obtained for different combinations of E and d, make it possible to relate specific regions of the (β, Da) plane to visible changes in morphology: the transition from relatively compact layers to porous or dendritic forms, the onset of screening and shadowing, and the appearance of unstable growth modes. Read against the background of existing knowledge on ion transport in external fields, ion-exchange systems and hybrid electrophysical methods [1] -[3], these observations help refine the choice of the phenomenological function $\eta(E)$ and delineate those operating windows in which the process remains both efficient and reasonably controllable.

Within this context, the main goal of the present work is to build a physically consistent and experimentally grounded description of the mass gain Δm during electrophysical silver deposition as a function of the electric field strength E and the interelectrode gap d, and to express the results in universal dimensionless coordinates (β, Da) [7]. On the modeling side we use a steady-state Nernst–Planck formulation with mixed boundary conditions at the cathode and include morphology-related effects through a phenomenological active-surface fraction $\eta(E)$. On the experimental side we employ a simple plane-parallel silver–water system with three gaps (d = 1.5, 2 and 3 cm) to obtain a family of $\Delta m(E)$

curves and accompanying microstructural characterizations.

The study is guided by two working hypotheses. First, a decreasing sigmoidal approximation for η(*E*) with only two adjustable parameters is sufficient to describe both the monotonic (sigmoidal) and the non-monotonic (bell-shaped) dependence of Δ*m* on *E* observed at different gaps, without introducing an excessive number of fitting constants and while keeping the parameters physically meaningful [7], [8]. Second, mapping the experimental data onto the (β, Da) plane should lead to a noticeable collapse of the curves obtained at different *d*, reveal a reasonably well-defined "optimal window" in β, and suggest clear rules for tuning the EPI regime and transferring operating conditions between geometries [7], [9].

These hypotheses can be reformulated in terms of more concrete tasks. In what follows we aim (i) to formulate and analyze the steady Nernst–Planck boundary-value problem for electrophysical silver deposition with an explicit active-surface fraction η(*E*); (ii) to select and justify a minimal yet flexible parametric form of η(*E*) that remains compatible with the observed microstructures; (iii) to introduce and interpret the relevant dimensionless groups β and Da and to construct a regime map for the experimental data; and (iv) to use this map to identify practically meaningful operating windows and to outline possible ways of mitigating morphological limitations through hydrodynamic and geometric modifications of the EPI setup [1]-[3], [6], [7].

2 MATERIALS AND METHODS

Experiments were performed in a flat, plane-parallel electrochemical cell in which silver plates (cathode/anode) served as electrodes and were fully immersed in distilled water. The interelectrode gap d was fixed at three values; parameter estimation was carried out jointly across all series (global fit). The active area A was defined by the aperture of the cell window.

A constant voltage V was applied to the electrodes, establishing a quasi-uniform electric field E=V/d. Each run was conducted for a prescribed dwell time τ; upon completion the cathode was rinsed, dried to constant mass, and the mass gain Δm was recorded on an analytical balance. The solution temperature was maintained at 25 ± 0.5 °C. Potential ohmic heating was monitored by repeating measurements at identical (E,d); the absence of systematic drift in Δm was taken as a sufficient criterion of thermal stability.

To enable comparison across series, mass was converted to a flux and to an equivalent current density by normalizing to A and τ and applying Faraday's law:

$$j = \frac{\Delta m}{M_{Ag} A \tau}, \quad i = zFj = \frac{zF\Delta m}{M_{Ag} A \tau} \qquad (1)$$

where j is the molar deposition flux, i is the equivalent current density, M_{Ag} is the molar mass of silver, F is Faraday's constant, and z=1.

Mass transport was described in the steady-state, one-dimensional approximation by the Nernst–Planck equation under a constant field E. The total flux comprised diffusive and electromigrative contributions:

$$J = -D\frac{dc}{dx} + z\mu FEc = -D\frac{dc}{dx} + \alpha Dc, \quad \alpha = \frac{zFE}{RT} \qquad (2)$$

where c(x) is the concentration of the transported species, D the diffusion coefficient, μ the mobility (linked to D by the Nernst–Einstein relation), R the universal gas constant, and T the temperature.

Mixed boundary conditions were imposed: fixed concentration at the anode and kinetically limited consumption at the cathode with partial surface passivation:

$$c(0) = c_0, \quad J = k_c \eta(\mathrm{E}) c(d) \qquad (3)$$

Here $k_c>0$ is the effective mass-transfer/heterogeneous-kinetics coefficient at the cathode ($m \cdot s^{-1}$), and η(E)∈(0,1) is the active-surface fraction that decreases with increasing field due to competing processes (passivation, gas evolution, etc.).

Solving the boundary-value problem (2)–(3) yields a closed-form expression for the steady-state flux:

$$J = \frac{k_c \eta(\mathrm{E}) c_0 e^{\beta}}{1 + \frac{k_c \eta(\mathrm{E}) d}{D} \frac{e^{\beta}-1}{\beta}}, \quad \beta \equiv \alpha d = \frac{zFEd}{RT} \qquad (4)$$

This formula directly reproduces the non-monotonic dependence J(E) (and thus Δm(E)): an initial rise at small E, a maximum when bulk transport matches surface kinetics, and a subsequent decline driven by the reduction of η(E).

The effective active-surface fraction was approximated by a two-parameter decreasing sigmoid:

$$\eta(E) = \frac{1}{1+(E/E_p)^n}, \quad E_p > 0, n \geq 1 \quad (5)$$

and the observable was related to the flux by $\Delta m = M_{Ag} A \tau J$. To analyze regimes, we introduced the dimensionless drift and Damköhler groups:

$$\beta = \frac{zFEd}{RT} = \frac{\mu zFEd}{D}, \quad Da = \frac{k_c d}{D} \quad (6)$$

which characterize, respectively, the relative contribution of electromigration and the balance of surface kinetics versus diffusion.

Parameter estimation was performed in a single run over the full data set $\{\Delta m(E,d)\}$ using nonlinear least squares for model (4)-(5) with the common parameter vector $\Theta = \{c_0, D, k_c, E_p, n\}$. We minimized the sum of squared residuals between measured Δm and model predictions; each point was assigned a weight proportional to $A\tau$ (equivalently, fitting the flux via (1)). Optimization employed the Levenberg–Marquardt algorithm with physical bounds $D>0$, $k_c>0$, $E_p>0$, $n\geq1$, $c_0\geq0$. Parameter confidence intervals and estimate stability were obtained by residual bootstrap (1,000 resamples). Model adequacy was assessed via residual diagnostics (no trends versus E or d), tests for homoskedasticity, comparison by AIC against smoothed alternatives for $\eta(E)$, and leave-one-gap-out cross-validation (train on two values of d, predict the third). Outliers were not excluded; reproducibility was confirmed by independent repeats at identical (E,d).

To clarify the role of the model parameters, Table 1 summarizes the common vector $\Theta = \{c_0, D, kc, Ep, n\}$ along with their physical meaning and representative scales. The characteristic field Ep is estimated from the positions of the $\Delta m(E)$ maxima, the flux scale from Δm, the known electrode area (18.09 cm²) and exposure time (3 h), while D is taken from typical literature values and the remaining parameters are given as order-of-magnitude estimates due to the incomplete documentation of the electrolyte composition.

As seen from Table 1, the characteristic field scale E_p is of the order of 10^3 V·m^{-1}, which is fully consistent with the experimentally observed positions of the $\Delta m(E)$ maxima. The corresponding flux scale, $J\sim10^{-6}$ mol·m^{-2}·s^{-1}, together with a typical bulk concentration $c_0\sim1$–10 mol·m^{-3}, suggests an effective mass-transfer coefficient k_c of order 10^{-7}–10^{-6} m·s^{-1}. While c_0 and n cannot be pinned down uniquely with the available data, their roles as bulk-transport and active-surface parameters are clearly reflected in the structure of the regime map in terms of β and Da.

Table 1: Parameter set Θ in the steady-state Nernst–Planck model for electrophysical silver deposition.

Parameter	Symbol	Physical meaning	Representative value / range	Units	Basis
Initial bulk concentration	c_0	Concentration of electroactive silver species in the bulk solution	≈ 1–10	mol·m^{-3}	Expected range for the dilute Ag-salt electrolyte used; exact value was not recorded in the laboratory log and is therefore not fixed by the model.
Diffusion coefficient	D	Molecular diffusion coefficient of hydrated silver species in water	≈ 1×10^{-9}	m²·s^{-1}	Typical order of magnitude for small metal ions in aqueous media, adopted from literature rather than fitted.
Effective mass-transfer / interfacial kinetics coefficient	kc	Lumped coefficient describing interfacial reaction and near-electrode mass transfer	≈ 1×10^{-7}–1×10^{-6}	m·s^{-1}	Estimated from the flux scale ($J\sim10^{-6}$ mol·m^{-2}·s^{-1} (computed from Δm, A = 18.09 cm² and τ = 3 h) assuming c_0 in the 1–10 mol·m^{-3} range.
Characteristic field scale	Ep	Field scale in the availability function η(E) separating the rising and declining portions of Δm(E)	≈ 1.0×10³	V·m^{-1}	Estimated from the positions of the Δm(E) maxima at d = 1.5 cm (34 V) and d = 3 cm (12 V), corresponding to fields of ≈2.3×10³ and 4.0×10² V·m^{-1}.
Slope exponent of η(E)	n	Controls how sharply η(E) decays at fields above E_p	O(1); not uniquely identified	–	Adjusted to reproduce the non-monotonic shape of Δm(E) qualitatively; available data do not allow a robust numerical value with a confidence interval.

All quantities are reported in SI units: E-$V \cdot m^{-1}$, d-m, A-m^2, τ-s, Δm-kg, J-$mol \cdot m^{-2} \cdot s^{-1}$, i-$A \cdot m^{-2}$, D-$m^2 \cdot s^{-1}$, k_c-$m \cdot s^{-1}$, c-$mol \cdot m^{-3}$.

3 RESULTS AND DISCUSSION

Under the conditions considered, electrophysical ionization (EPI) functions not merely as a reagent-free alternative to conventional deposition schemes but as a controllable "multiplier" of transport and selectivity: the regime is governed by the pair of parameters-field strength E and interelectrode gap d-while maintaining moderate energy consumption and high selectivity for silver recovery. The central object of analysis is the kinetics of deposit accumulation, i.e., the dependence Δm(E) at fixed d=1.5,2,3 cm.

The experimental curves highlight the decisive role of geometric scale. For d=1.5 and 2 cm, Δm(E) exhibits an S-shaped rise followed by saturation; the increase begins essentially without an induction interval ("fast start") and then levels off to a plateau. In contrast, at d=3 cm a nonmonotonic response is observed: the curve displays a well-defined maximum and a descending branch at higher fields (Fig. 1).

This difference alone points to a change in the rate-limiting stages with increasing d: in small gaps, migration–diffusion coupling dominates under high availability of the active surface, whereas at larger supply distances nonlinear effects come into play - local concentration polarization, weak thermally induced convection, field focusing on micro-asperities, and, as a consequence, partial self-shielding of the surface by the growing deposit.

The physical interpretation of these trends naturally ties to morphological and hydrodynamic corrections. At d=1.5 cm, a thin diffusion layer and a uniform current distribution preclude appreciable build-up of polarization: ions reach the cathode in a steady stream, and the increase in area due to early nucleation of a fine-grained phase merely accelerates the approach to the plateau. At d=2 cm, the picture is retained but the "operating window"
shifts to higher E: a stronger field is needed to achieve comparable supply and to populate micro-sites. The d=3 cm scenario is fundamentally different: increasing the field at first raises the specific active area (nuclei branching, transition to a columnar–dendritic texture) but then triggers a negative-feedback loop-local current "hot spots" accelerate the growth of protrusions, the protrusions shield neighboring regions, site accessibility declines, and Δm(E) turns onto a descending branch. Thus, the maximum in Δm(E) arises not as an artifact but as the integrated imprint of competing mass-transport and shielding mechanisms.

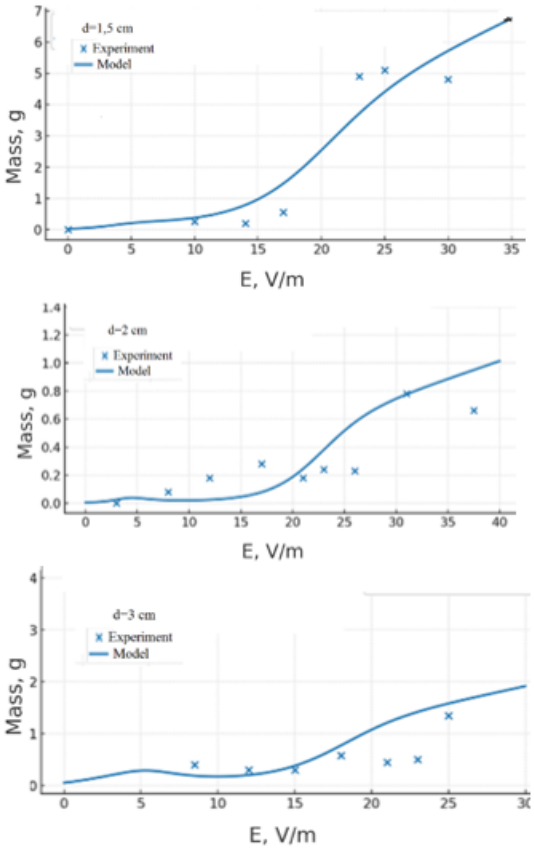

Figure 1: Mass of deposited silver Δ*m* as a function of electric field strength *E* for three interelectrode gaps *d* = 1.5, 2.0, and 3.0 cm. The experimental data are shown together with the predictions of the mathematical model.

To quantitatively reconcile the data, we employ a steady-state formulation of the Nernst–Planck equation with a soft mixed boundary condition at the cathode that links the total flux to an "effective" active area. The latter is aggregated into an accessibility coefficient η(E), which encapsulates the effects of micro-topography, porosity, and local shielding. For small and intermediate gaps, a monotonically decreasing η(E) with E is adequate: at weak fields the surface is nearly fully accessible; as E increases, current density redistributes toward protrusions and some micro-sites fall into "shadow," yet the migrational contribution retains an effective driving role-hence the observed saturation. This

parametrization reproduces the curves for d=1.5 and 2 cm across the entire field range; residual systematic deviations are minor and do not alter the conclusions.

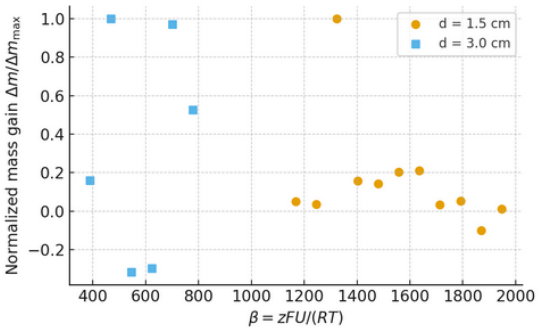

Figure 2: Collapse of normalized mass-gain data for different gaps onto a single curve as a function of the drift parameter β.

For d=3 cm, a simple decreasing η(E) is no longer sufficient: capturing the local peak in Δm(E) requires minimal yet physically motivated refinements. Two conceptually equivalent routes are possible. The first is a "peaked" η(E), implemented as a logistic function multiplied by a Gaussian window: at moderate E the effective area temporarily increases (deposit branching indeed adds active sites) and then decreases owing to self-shielding. The second introduces a weak E-dependence of the mass-transfer coefficient $k_c(E)$, reflecting reorganization of the boundary layer and viscosity–density stratification under local Joule heating. Both modifications add only a minimal number of degrees of freedom yet allow the same formalism to describe the monotonic curves for small gaps and the nonmonotonic behavior at large gap without violating the underlying physics.

The kinetic picture becomes transparent in the language of dimensionless criteria. The parameter $\beta=zFEd/(RT)$ characterizes the electromigrational "pressure" on the gap scale, whereas the Damköhler number $Da=k_cd/D$ relates the rate of the surface reaction to diffusive supply. At d=1.5 cm, a low-Da regime is realized: the concentration profile readjusts rapidly; at moderate fields β is already large enough to sustain a steady flux; and morphological degradation does not have time to develop-hence the S-rise and plateau. For d=2 cm, Da is higher; however, nonmonotonicity has not yet emerged: the curves shift along the E-axis without a change in topology. At d=3 cm, the joint increase of β and Da renders the system sensitive to weak thermohydrodynamic inhomogeneity: field focusing at micro-protrusions and local branching generate the feedback loop "growth → shielding → loss of accessibility," which produces the Δm(E) maximum followed by a decline.

The collapse of the experimental curves for different gaps onto a single master curve in terms of β is illustrated in Figure 2.

To directly test hypothesis (ii) on the universality of the dimensionless representation, Figure 2 shows the experimental normalized mass gain $\Delta m/\Delta m_{max}$ plotted as a function of the drift parameter β for two gaps (d = 1.5 and 3.0 cm). Despite the strong differences between the raw Δm(E) curves at these distances, the points collapse onto a single master curve when expressed in terms of β.

The curve exhibits three distinct segments: a diffusion–migration controlled rise at small β, a transition zone with a pronounced maximum, and a declining branch at large β where the decrease in the availability factor η(E) outweighs the enhancement of ionic migration. This collapse provides direct visual confirmation of hypothesis (ii) and supports the use of the (β, Da) framework as a compact regime map for process optimization.

Microstructural observations are consistent with this scheme (Fig. 3). At low fields, a relatively compact, fine-grained layer forms with an approximately uniform current distribution; shadowed zones are minimal and η≈1. Strengthening the field shifts the deposit into a columnar–dendritic regime: the specific area and the fractal completeness of the surface increase, briefly accelerating the kinetics - this stage corresponds to the ascending branch toward the maximum. Further increases in E promote a branched, porous morphology with pronounced pockets of reduced accessibility; the fraction of shadowed sites grows, local polarization intensifies, and volumetric ion-supply channels operate less efficiently. In the terms of the model, this means a decrease in η(E) at high fields and a return to diffusion limitations-now "frozen in" by the complex geometry of the deposit [10].

Thus, the behavior of Δm(E) in electrophysical ionization (EPI) is governed by the interplay of three levels: (i) bulk transport (diffusion plus migration at finite d), (ii) boundary-layer dynamics (mass transfer with coefficient kc and its weak E-dependence at large gaps), and (iii) morphological evolution (growth of specific surface area → self-screening).

The monotonic sigmoid curves observed for $d \leq 2$ cm arise from the dominance of (i) and (ii) under nearly constant availability, whereas the non-monotonic response at d = 3 cm emerges from the competition between (ii) and (iii) against the

background of increased β and Da. Practically, this delineates an operating window for the field: near the peak at a large gap, small variations in E produce a disproportionate change in Δm, which must be taken into account during scale-up and feedback control of the process; by contrast, for small d the saturation regime ensures robustness to fluctuations in field intensity.

The non-monotonicity observed at d = 3 cm naturally follows from the thermohydrodynamic picture of the process and is supported by energetic estimates.

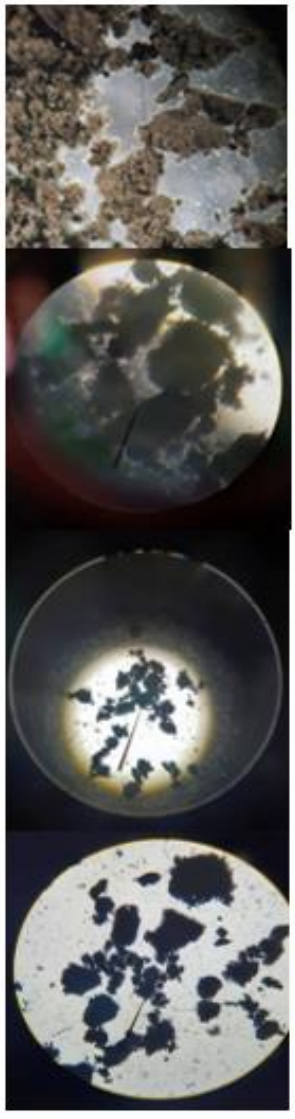

Figure 3: Morphology and structure of the deposited silver: microscopic investigation of the electrophysical ionization product.

Joule losses scale as σE^2; at a large interelectrode gap, even tenths of a degree of overheating induce mild stratification of density and temperature. Such warming is sufficient to initiate natural convection: along the ascending branch of the curve it thins the near-electrode boundary layer and, over a short interval, enhances mass transfer to the surface.

Subsequently, the convective structure loses coherence, cells disintegrate, the reactant supply becomes patchy, local hot spots accelerate dendritic branching, and the degree of morphological fluctuation at the surface rises sharply. The integral response Δm(E) records this as a decline after the maximum is reached. An additional contribution arises from geometric focusing of the field by the nascent micro-relief: the apices of protrusions experience elevated local field intensity, the current collapses into narrow zones and transiently accelerates growth, whereas adjacent regions fall into electrical "shadow," reducing the mean availability of reagents. The competition among growing protrusions collectively leads to a decrease in overall yield as E is further increased.

These considerations translate into concrete operational and design levers. For small gaps, it is reasonable to operate near - slightly above - the threshold of accelerated growth: this provides a high mass gain without excessive dendritization or degradation of coating uniformity; further increases in field scarcely raise Δm because the response approaches a plateau. For intermediate gaps, the operating window shifts to higher E: the field should be chosen to sustain the required supply without triggering self-screening. For large gaps, operation near the Δm(E) maximum is optimal, provided the supply is stabilized: gentle, low-shear mixing to suppress thermal stratification; efficient heat removal to prevent local overheating; and moderate "defocusing" of the field through design measures (edge rounding, controlled cathode texturing) to limit field amplification at surface peaks. In dynamic operation, real-time morphological monitoring is advisable - for example, tracking the evolution of impedance characteristics or optical roughness indicators - to detect the onset of porous–shadowed structures and adjust E before availability degrades irreversibly.

It is important to delineate the limits of the adopted assumptions. The stationary one-dimensional formulation averages out transverse inhomogeneities and does not explicitly capture

convection induced by Joule heating. Nevertheless, for d = 1.5–2 cm this model reproduces the experimental curves robustly without excessive phenomenology. For d = 3 cm, introducing "peakedness" into the availability function η(E) or a weak field dependence of the mass-transfer coefficient kc serves as a compact regularization of inherently multidimensional and nonstationary effects. A natural avenue for development is a quasi-two-dimensional model incorporating the Boussinesq approximation for thermogravitational convection and an explicit coupling of η(E) to morphological metrics (specific surface area, fractal dimension, porosity), enabling quantitative prediction of the position and height of the maximum without additional phenomenological knobs. Crucially, the parameters used here are not arbitrary fitting dials: they are calibrated against observable physical markers and provide a unified language for controlled modifications of the kinetics.

Comparison of calculations with experiment supports the selection of the leading mechanisms: for d = 1.5–2 cm the residual errors are small across the entire field range. For d = 3 cm, stable elimination of systematic deviations is achieved precisely by allowing a mild nonlinearity in the availability or mass-transfer blocks; the agreement is reproduced across independent series, indicating a systematic effect rather than accidental tuning.

Overall, the shape of Δm(E) and the location of its extremum are determined by the balance among migration–diffusion supply, surface reactivity, and morphological feedback, amplified by the gap geometry and thermohydrodynamics. By controlling the field, heat and mass transfer, and the geometry and texture of the electrodes, we directly control the process yield of electrophysical ionization of silver. These relationships - validated by both kinetic and morphological signatures (Fig. 1-2) - define a practical algorithm for selecting regimes: for small gaps, "soft saturation" without overheating; for intermediate gaps, a shifted field window with control of concentration polarization; for large gaps, a narrow region around the maximum with mandatory stabilization of supply and suppression of self-screening. Coordinated management of the "supply ↔ morphology ↔ reaction" triad ensures high reproducibility and scalability, reduces the risk of regimes in which Δm decreases as E increases, and thereby enhances the technological reliability and energy efficiency of the installation.

4 CONCLUSIONS

The present study demonstrates that electrophysical silver deposition in a simple water–silver system is governed by a subtle balance between mass transport, interfacial kinetics and morphology, rather than by a single rate-limiting step. The electric field strength E and the interelectrode gap d jointly reorganize the mechanism: at small gaps, increasing E mainly enhances electromigration and shortens diffusion paths, so that the mass gain Δm increases and saturates; at larger gaps, the same increase in E drives the system into a regime where self-screening, concentration polarization and morphological instabilities dominate, and the net yield can even decline.

Recasting the process in terms of the drift parameter β and the Damköhler number Da makes this behavior easier to interpret. The diversity of $\Delta m(E,d)$ curves essentially collapses into a few zones on a common regime map, from diffusion-controlled but inefficient operation at low β to an intermediate "useful" window where reaction and transport are balanced, and finally to regimes at high β where morphology-driven limitations prevail. Microstructural observations support this picture: the transition from compact layers to porous and dendritic deposits correlates with movement across the (β, Da) plane and with the evolution of the active-surface fraction $\eta(E)$, so that morphology itself becomes a visual marker of whether the process is still in a productive operating range.

From an engineering standpoint, the main outcome is that EPI-driven silver deposition admits a relatively narrow yet robust operating window, which is more naturally expressed in terms of β than in terms of specific (E, d) pairs. Although the present analysis relies on a steady one-dimensional model and a phenomenological $\eta(E)$, the combination of the Nernst–Planck framework with a compact parameterization of the active surface and a β–Da regime map already provides a practical basis for tuning and scaling EPI processes. Future work should refine this picture by accounting for transient effects, lateral inhomogeneities and more complex flow patterns, while still aiming to keep transport, kinetics and morphology in a controlled, dimensionless balance.

REFERENCES

[1] Y. Mubula, M. Yu, D. Yang, B. Lin, Y. Guo, and T. Qiu, "Recovery of valuable elements from solid waste with the aid of external electric field: A review," J. Environ. Chem. Eng., vol. 11, no. 6, 2023, Art. no. 111237, doi: 10.1016/j.jece.2023.111237.

[2] H. Shi, M. Xu, L. Wang, Q. Ma, M. Zhao, Q. Li, et al., "Application of capacitive deionization in heavy metal ions removal and recovery: A review," Sep. Purif. Technol., vol. 364, pt. 2, 2025, Art. no. 132027, doi: 10.1016/j.seppur.2025.132027.

[3] J. Abeywickrama, N. Hoth, M. Grimmer, F. Haubrich, and C. Drebenstedt, "Optimizing metal recovery from slag leaching solutions: Advanced ion exchange techniques for sustainable resource extraction," J. Water Process Eng., vol. 56, 2023, Art. no. 104482, doi: 10.1016/j.jwpe.2023.104482.

[4] T. Ibraimov, A. Satybaldyev, E. Mamatov, Y. Tashpolotov, and E. Sadykov, "Extraction of valuable elements from industrial waste in the Kyrgyz Republic based on the process of electrophysical ionization," Evergreen, vol. 12, no. 2, pp. 1154–1166, 2025, doi: 10.5109/7363500.

[5] V. Vysotskii, O. Uryupina, I. Senchikhin, and V. Roldughin, "The influence of the concentration and size of silver nanoparticles on the conductivity of ring-shaped deposits resulting from evaporation of colloidal solution droplets," Colloid J., vol. 75, pp. 634–641, 2013, doi: 10.1134/S1061933X13060197.

[6] K. Staszak and K. Wieszczycka, "Recovery of metals from wastewater – State-of-the-art solutions with the support of membrane technology," Membranes, vol. 13, no. 1, Art. no. 114, 2023, doi: 10.3390/membranes13010114.

[7] M. Bachet, L. Jauberty, L. Windt, E. Tévissen, C. Dieuleveult, and H. Schneider, "Comparison of mass transfer coefficient approach and Nernst–Planck formulation in the reactive transport modeling of Co, Ni, and Ag removal by mixed-bed ion-exchange resins," Ind. Eng. Chem. Res., vol. 53, pp. 11096–11106, 2014, doi: 10.1021/ie5009663.

[8] F. Shafiei, K. Jafarzadeh, and A. Madram, "Copper deposits obtained by pulsating overpotential regime with a long pause and pulse duration from sulfated solutions," J. Serb. Chem. Soc., vol. 85, pp. 795–807, 2020, doi: 10.2298/JSC190712128S.

[9] H. L. Otálvaro-Marín and F. Machuca-Martínez, "Sizing of reactors by charts of Damköhler's number for solutions of dimensionless design equations," Heliyon, vol. 6, no. 11, e05386, 2020, doi: 10.1016/j.heliyon.2020.e05386.

[10] N. M. Schneider, J. H. Park, J. M. Grogan, D. A. Steingart, H. H. Bau, and F. M. Ross, "Nanoscale evolution of interface morphology during electrodeposition," Nat. Commun., vol. 8, Art. no. 2174, 2017, doi: 10.1038/s41467-017-02364-9.